2-1-2019

Human and natural controls on erosion in the Lower Jinsha River, China

Amanda H. Schmidt
Oberlin College

Alison R. Denn
University of Vermont

Alan J. Hidy
Lawrence Livermore National Laboratory

Paul R. Bierman
University of Vermont

Ya Tang
Sichuan University

LAWRENCE
LIVERMORE
NATIONAL
LABORATORY

LLNL-JRNL-751018

Human and natural controls on erosion in the Lower Jinsha River, China

A. H. Schmidt, A. R. Denn, A. J. Hidy, P. R. Bierman, Y. Tang

May 8, 2018

Journal of Asian Earth Sciences

Disclaimer

For submission to the Journal of Asian Earth Sciences

26 September 2018

Human and natural controls on erosion in the Lower Jinsha River, China

Amanda H. Schmidt[1*], Alison R. Denn[2], Alan J. Hidy[3], Paul R. Bierman[2], Ya Tang[4]

1: Geology Department, Oberlin College, Oberlin, OH 44074

2: Department of Geology, University of Vermont, Burlington, VT 05405

3: Center for Accelerator Mass Spectrometry, Lawrence Livermore National Laboratory, Livermore, CA 94550

4: Department of Environment, Sichuan University, Chengdu, China

* Corresponding author: aschmidt@oberlin.edu

Abstract

The lower Jinsha River has the highest sediment yield rates of the entire Yangtze watershed; these high yields have previously been attributed to a mix of the local geologic setting as well as intensive human land use, particularly agriculture. Prior studies have not quantified long-term background rates of sediment generation, making it difficult to know if modern sediment yield is elevated relative to the long-term rate of sediment generation.

Using *in situ* ^{10}Be in detrital river sediments, we measured sediment generation rates for tributaries to the lower Jinsha River. We find that the ratio of modern sediment yield to long-term sediment generation rate is 5.9 ± 2.8 (mean, 1 SD, n = 5), which is significantly higher than that elsewhere in western China and implies contemporary rates of sediment export far exceed long-term rates of sediment generation by weathering on hillslopes (1.9 ± 0.9 [median, 1 SD, n = 20]; (Schmidt et al., 2017)). Long-term (thousand year) rates of sediment generation correlate best with the steepness of the upstream watershed, a result found around the world. In contrast, modern sediment yield and the ratio of sediment yield to sediment generation rates correlate best with agricultural land use and distance to the nearest dam. Modern (1950s-1980s) sediment yield and the ratio of sediment yield to sediment generation also correlate well with percent of the watershed containing landslides observable today. The significantly higher modern sediment yield, lack of correlation between percent of the basin with landslides and long-term rates of sediment generation, and widespread deforestation and agriculture in the region suggest that landslide scars observable today are at least in part a result of human-induced land use change. Thus, we conclude that a mix of geologic setting and human activity control high contemporary sediment yield rates in the region.

Keywords: ^{10}Be, landslides, erosion, Yangtze River, sediment yield

Highlights

- Long-term sediment generation rates scale with mean basin slope throughout the lower Jinsha River
- The ratio of contemporary sediment yield to long-term sediment generation is average of five
- People are raising sediment yield with agriculture and deforestation and lowering it with dams
- Percent of basins with landslides is positively correlated to modern sediment yield

1. Introduction

Human activity in the environment can change the movement of sediment across the landscape in varying ways, depending on the scale of the disturbance, size of the watershed, and type of disturbance (Syvitski et al., 2005). For example, widespread construction of dams can greatly reduce the load of sediment in rivers and agriculture and deforestation can increase erosion on hillslopes and often increases sediment yield in rivers (Hewawasam et al., 2003). In areas with high natural erosion rates, large volumetric contributions of landslides to the long-term sediment budget, and tectonically active geologic settings, it can be difficult to discern the relative increase in erosion caused by human activity (National Research Council, 2010). Landslide frequency and distribution can also be strongly influenced by human activity, including deforestation and road building (Benda and Dunne, 1997; Bierman et al., 2005). Without both long-term rates of sediment generation (often calculated using *in situ* ^{10}Be in detrital river sediment (Bierman and Steig, 1996; Brown et al., 1995; Granger et al., 1996)) and modern sediment yields (from river gauging stations records in the region), it is difficult to compare short-term sediment yields influenced by human action to long-term sediment generation rates controlled by geologic factors (e.g., Kirchner et al., 2001).

In western China, prior studies find that human activity, in particular agricultural land use, has increased sediment yield relative to long-term rates of sediment generation by approximately a factor of two (Schmidt et al., 2017). The lower Jinsha River, east of the regions previously studied in China (Chappell et al., 2006; Schmidt et al., 2017; Schmidt et al., 2011), has long been identified as a region with unusually high contemporary rates of erosion and sediment yield (Jiang et al., 2015; Lu, 2005). These elevated erosion and sediment yield rates are typically

blamed on the effects of land use by humans (Jiang et al., 2015; Lu, 2005). However, prior research only considers short-term sediment yield and erosion data rather than considering long-term background rates of sediment generation as a baseline by which to evaluate the contemporary data. In this paper, we consider the dual effects of geologic setting and human activity in setting the ratio of modern sediment yield to long-term rates of sediment generation in the lower Jinsha River region of the Yangtze River watershed.

2. Background

In situ-produced ^{10}Be ($^{10}Be_i$), measured in fluvial sediment, has been used extensively to quantify rates of erosion and infer background rates of sediment generation mostly, but not exclusively, in small, headwater basins. $^{10}Be_i$ concentration in detrital sediment is inversely related to erosion rate (Bierman and Steig, 1996; Brown et al., 1995; Granger et al., 1996) and erosion and sediment generation rates calculated from measured $^{10}Be_i$ concentration are insensitive to human activities if depth of erosion is shallower than the mixed soil layer (~100 cm) (Bierman and Steig, 1996; Brown et al., 1995; Brown et al., 1988; Granger et al., 1996; Reusser et al., 2015; Schmidt et al., 2016; Vanacker et al., 2007; Von Blanckenburg et al., 2004).

Many prior studies compare modern sediment yield with long-term sediment generation rates to understand if and how people are altering erosion and sediment supply to rivers (e.g., Covault et al., 2013; Kirchner et al., 2001). When modern sediment yield and long-term sediment generation are similar (e.g., ratio ~ 1), the landscape is interpreted as being in mass steady state (Matmon et al., 2003; Wittmann et al., 2011). When modern sediment yield is significantly higher than long-term rates of sediment generation (ratio > 1), land use changes are blamed for increasing contemporary sediment yield (Hewawasam et al., 2003; Reusser et al.,

2015; Schmidt et al., 2017); this effect is more commonly seen in smaller watersheds (Vanmaercke et al., 2015). If long-term rates of sediment generation significantly exceed modern sediment yield (ratio < 1), then the data are interpreted as dams reducing modern sediment yield (Syvitski et al., 2005), rare but important sediment transport events being missing by short contemporary records (Kirchner et al., 2001; Tomkins et al., 2007), and dams raising apparent $^{10}Be_i$-derived sediment generation rates through selective sourcing of sediment from below the dam (Reusser et al., 2017).

Prior work in China has focused on major Yangtze tributaries (Chappell et al., 2006) and western Sichuan/eastern Tibet (Schmidt et al., 2017; Schmidt et al., 2011). The Yangtze tributaries have ratios of contemporary sediment yield to long-term rates of sediment generation from 0.2 to 2.3 (mean = 0.8 ± 0.5, n = 6) (Chappell et al., 2006) and a study of the main stem of the Yangtze, Mekong, and Tsang Po rivers finds that only the Yangtze River has a ratio greater than one (1.26), while the Mekong and Tsang Po rivers have ratios of 0.57 and 0.20, respectively (Schmidt et al., 2011). The low ratios for the Mekong and Tsang Po are attributed to stochastic events such as landslides driving the long-term patterns of sediment generation but not being captured in the short-term sediment yield data (Schmidt et al., 2017). In contrast, in a large study of 20 gauging stations in Yunnan and eastern Tibet, the mean ratio of sediment yield to sediment generation is 1.9 ± 1.7 (Schmidt et al., 2017). The doubling of sediment yield compared to sediment generation is attributed to human agricultural land use (Schmidt et al., 2017).

3. Study area

The lower Jinsha River is the region of the Yangtze River upstream of the confluence with the Min River and downstream of the confluence with the Yalong River (Figure 1); the river

97 forms the divide between Sichuan (to the north/west) and Yunnan (to the south/east) in this
98 region. The study area is upstream of the Sichuan basin and appears to have a knickpoint moving
99 through the system (Figure 2, 3), possibly due to the formation of the Sichuan basin. In the
100 uppermost basins of the study area, the topography is rolling and the Jinsha flows through a wide
101 open valley. In the middle of the study area, the Jinsha is incised into a deep gorge inset into
102 rolling topography. In the downstream reaches of the study area, the landscape is steep and
103 deeply dissected.

104 A series of four dams are being built along the main stem of the lower Jinsha River,
105 which will collectively store 41.3 billion cubic meters of water and generate nearly double the
106 electricity produced by the Three Gorges Dam (38 GW compared to 18.2 GW) (Yao et al., 2006).
107 At the time of sampling, the lower two dams had been closed (Xiangjiaba and Xiluodu) while the
108 upper dams (Wudongde and Baihetan) were still under construction. Numerous small dams,
109 which likely trap sediment, dating back to the 1950s are present in most tributary valleys (Lu,
110 2005).

111 Agriculture in the region is concentrated on less steep slopes, so there is an inverse
112 correlation between agricultural land use and steepness ($R^2 = 0.50$, $p < 0.05$) (Figure 1). Up to 42%
113 of the basins sampled are agricultural in land use (mean = 30%, minimum = 13%). The
114 remaining area is a mix of primarily forest and grassland (basins are up to 72% forested [mean =
115 43%, minimum = 13%] and up to 50% grassland [mean = 25%, minimum = 8%]), although there
116 are some significant lakes (one is nearly 3% of the area of one large basin; other basins are <0.5%
117 water), urban areas (including Kunming, which accounts for >3% of one basin area; other basins
118 are up to ~1% urban [mean = 0.6%]), and shrublands (up to nearly 5% [mean = 1.4%, minimum
119 = 0.07%]). Although commercial logging is now banned in western China and agricultural land

120 on sloping hillslopes is being reforested, this has only happened in the last ~20 years and prior to
121 the late 1990s; both logging and cultivation of steep land were common in western Sichuan (Trac
122 et al., 2007; 2013; Urgenson et al., 2010).

123 Rainfall varies little over the study area. Basins average 777 to 996 mm/yr of
124 precipitation with rainfall rates typically higher to the north of the river (in Sichuan) than to the
125 south (in Yunnan) (Yatagai et al., 2012). The climate is monsoonal and the vast majority of the
126 rain falls in the summer months (June, July, August, and September) (Yatagai et al., 2012). Mean
127 annual temperature in the study region is 15^{o}C, with maximum temperatures during the rainy
128 season (mean = 20^{o} C during this time) (Jiang et al., 2015). With the exception of one watershed
129 (JS09), the region is classified as temperate, dry winter, and either hot or warm summer. JS09 is
130 classified as Arid steppe hot (Peel et al., 2007).

131 One subcatchment we sampled, the Xiao River, is the site of the Dongchuan Debris Flow
132 Observatory, a field site for the Chinese Academy of Sciences State Key Lab for Mountain
133 Hazards Research (Zhou et al., 2016). This tributary to the Jinsha is considered to be the most
134 debris flow prone region in China due to a mix of local geology – a river flowing along fractured
135 rock in a tectonically active area – and human activity, including both mining and agriculture
136 (Wu et al., 2016).

137 Prior work in the region focused on modern rates of sediment yield and erosion. The
138 region is one of the highest sediment-producing areas of the Yangtze basin (Lu and Higgitt, 1998,
139 1999). Typical narratives assert that the mix of geologic setting and human activity (agriculture)
140 have caused the high rates of sediment yield (Jiang et al., 2015; Lu, 2005; Lu and Higgitt, 1998,
141 1999). One modeling study finds that highest rates of erosion are on agricultural slopes between

142 15^{o} and 35^{o}. Modelled erosion rates range from 500 to 15,000 tons/km^2-year; the mean in the
143 study region is 5210 tons/km^2-year (Jiang et al., 2015). Focusing on just one tributary of the
144 study area (the Longchuan River, the farthest west that we sampled), a study of discharge and
145 sediment yield reports that although soil erosion is severe in the watershed, sediment yield from
146 the watershed is <1000 tons/km^2-year because of widespread construction of reservoirs in
147 tributary valleys since the 1950s (Lu, 2005). However, they do find a significant increase in
148 sediment yield in the lower reaches of the watershed, which they attribute to human activity (Lu,
149 2005). In addition, prior analysis finds that sediment yield has generally increased in agricultural
150 areas and decreased in urban areas over the period record for gauging station data (Lu and
151 Higgitt, 1998, 1999).

152 # 4. Methods

153 *4.1 Field methods*

154 During January 2016, we collected medium sand (250-850 μm) samples from the active
155 river channels of nine tributaries to the lower Jinsha River (Figure 1; Table S1); five are at or
156 near gauging stations with previously recorded sediment yield data (Lu and Higgitt, 1998, 1999).
157 Sites were pre-selected for watersheds that span a range of basin-average slope (15^{o} to 25^{o}) in
158 order to capture the range of variability in the region. Samples were collected from alluvial rivers
159 in landscapes with varying degrees of agricultural land use. River banks were typically not
160 agricultural, although agriculture on hillslopes in the basins is common. Although we did not see
161 active forestry operation, we observed few forests and many bare slopes. We also observed few
162 reforestation sites, even though the Returning Farmland to Forest Program had already been
163 going on for more than ten years (Trac et al., 2007; 2013; Urgenson et al., 2010). In addition,

hillslopes frequently had small, shallow landslides and little vegetation. Bedrock appears to be covered only with shallow regolith or at the surface in much of the study area. The main stem of the Jinsha River was being dammed with a series of large dams during the time we were doing field work. In the downstream reaches of the study area, dams were already closed and the main channel of the Jinsha was a series of large lakes. All samples were collected upstream of backwater from the dams. The results for one sample (JS11) is the error weighted average of two samples (JS10 and JS11) taken ~2 km apart from one another and processed separately.

4.2 Basin average parameters

We determined watershed boundaries using the 30 m GDEM topographic dataset (NASA LP-DAAC, 2012) and then used the same elevation dataset to extract effective elevation (Portenga and Bierman, 2011), average basin slope, and upstream area for each watershed. Rainfall data are taken from the APHRODITE dataset (Yatagai et al., 2012). This dataset is coarser than other available datasets for rainfall in the region, but has better spatial and temporal accuracy (Andermann et al., 2011). Land use was determined from the Global Land Cover (GLC) dataset (Chen et al., 2015).

The study area has frequent landslides (Wu et al., 2016). To quantify the area of landslides in the watersheds as a possible control on either long-term rates of sediment generation or modern sediment yield, we visually mapped landslide scars in Google Earth and then determined the percentage of each watershed that is covered by landslide source areas. The smallest landslide mapped is 22 m^2, suggesting that the limit to seeing and mapping landslides is ~20 m^2.

Carbonate rocks are common in the study area. We determined the extent of carbonate rocks from existing geologic maps (Figure 1D) (Burchfiel and Chen, 2012) and although up to

57% of watersheds are underlain by carbonate likely containing little or no sand-sized quartz (Table S2), these rocks are uniformly distributed across all elevations of the basins and the effective elevation used in determining basin average erosion rates does not change when we exclude areas underlain by carbonate rocks from the calculation.

4.3 $^{10}Be_i$ data

Quartz from the samples was isolated and purified through a series of acid etches using a modification of the method of Kohl and Nishiizumi (1992). $^{10}Be_i$ was extracted from quartz following the method of Corbett et al. (2016). Each batch contained one process blank and one CRONUS N standard (Jull et al., 2015). Once the quartz was dissolved in hydrofluoric acid, aliquots were removed and analyzed by inductively coupled plasma-optical emission spectroscopy (ICP-OES) to measure ^{9}Be content (Corbett et al., 2016; Portenga et al., 2015).

Isotopic ratios were measured using Accelerator Mass Spectrometry (AMS) at the Center for Accelerator Mass Spectrometry at Lawrence Livermore National Labs and normalized to the ICN 07KNSTD3110 standard with an assumed ^{10}Be/^{9}Be ratio of 2.85 x 10^{-12} (Nishiizumi et al., 2007) (Table S1). Background correction was done using full process blanks, one of which was run with each batch of 10 samples. Samples were processed in two batches at UVM with blank measurements of $6.20 \times 10^{-16} \pm 2.97 \times 10^{-16}$ and $2.17 \times 10^{-15} \pm 2.29 \times 10^{-16}$; blank measurements are at least 30 times lower than measured ratios in samples.

Background sediment generation rates [tons/km^2-yr] were calculated from $^{10}Be_i$ concentrations using the CRONUS Earth online erosion rate calculator version 2.3 using constants file 2.3 (http://hess.ess.washington.edu/) (Balco et al., 2008) (see table S3 for CRONUS input table). We calculated the effective elevation of each watershed using the

209 approach of Portenga and Bierman (2011) (Table DR2). We did not adjust calculations for
210 watersheds with dams, but recognize that this could result in overestimating sediment generation
211 rates for samples taken in close proximity to dams if those dams effectively restrict or cut off
212 sediment supply from upstream – something unknowable without extensive fieldwork and details
213 of the dam operations (Reusser et al., 2017). Erosion rates for samples taken a short distance
214 downstream of dams which cut off sediment supply have apparently higher erosion rates because
215 sediment is sourced from downstream of the dam, an area with a lower mean elevation than the
216 entire watershed including the area upstream of the dam. Because $^{10}Be_i$ production scales with
217 elevation and erosion rates scale inversely with $^{10}Be_i$ concentration, excluding high elevation
218 (and thus high $^{10}Be_i$ production) regions will lower concentration and artificially raise apparent
219 erosion rates (Reusser et al., 2017). We used the time-invariant scaling scheme of Lal (1991) and
220 Stone (2000) and the global production rate of $^{10}Be_i$ of 4.10±0.35 atoms/g-yr (Balco et al., 2008).

221 ## 5. Results and discussion

222 Using a combination of $^{10}Be_i$-derived sediment generation rates and previously published
223 sediment yield data for the region, we explore the relative influence of agricultural land use,
224 topography, and climate on the high sediment yield in the lower Jinsha River compared to other
225 parts of the Yangtze River system. In this section, we consider the controls on long-term rates of
226 sediment generation, modern sediment yield, and the ratio of sediment yield to sediment
227 generation. We then further compare our sediment generation data to a prior study modeling
228 hillslope erosion in the lower Jinsha River (Jiang et al., 2015). Given the small number of
229 watersheds we sampled in this study region, formal statistical tests have little power, especially
230 for the sediment yield values and the ratio of long-term sediment generation to short-term

231 sediment yield, where only five watersheds have data. However, qualitatively plots of such data
232 still provide qualitative insight into the behavior of the system. Quantitative statistical data are
233 available in the data repository (table DR5).

234 Long term, background sediment generation rates in the study region vary from 25 to 418
235 tons/km^2-yr (mean = 190±129 tons/km^2-yr, n = 9), but there are no systematic patterns of
236 through the study area (Figure 4A; table S4). These rates are slightly lower than sediment
237 generation rates measured to the west in the Mekong, Red, and Salween drainages (Schmidt et al.,
238 2017) and on the high end of those for other eastern tributaries to the Yangtze (Chappell et al.,
239 2006). Long-term rates of sediment generation correlate best with the distance to the first dam
240 upstream of the sample and the mean hillslope steepness in the watershed (Figure 4); both are
241 positive correlations. In studies elsewhere, distance to dams is inversely correlated with erosion
242 rates (and sediment generation rates) because dams bias sediment to come from lower altitude
243 locations with lower $^{10}Be_i$ production rates (Reusser et al., 2017). We interpret the positive
244 correlation with distance to dams as an indication that both higher sediment generation rates and
245 dams are found in steeper areas.

246 The positive correlation between the hillslope steepness in the upstream watershed and
247 sediment generation rates suggests that steeper hillslopes typically have higher rates of sediment
248 generation, a result that has been found in other studies using $^{10}Be_i$ to derive sediment
249 generation and erosion rates (as summarized in Portenga and Bierman, 2011). This could be
250 related to the knickpoint moving through the region – high, flat, and undissected parts of the
251 watershed are less likely to have dams and likely to have lower erosion rates, while incised and
252 steeper parts of the watersheds are more likely to have both dams and higher erosion rates.

Five of the basins also have sediment yield data (1950s-1987) from Chinese gauging stations (Lu and Higgitt, 1998, 1999), which vary from 624 to 2792 tons/km^2-yr (mean = 1297±873 tons/km^2-yr, n = 5). These data were collected during a period of expanding agriculture and deforestation throughout China (Schmidt et al., 2011). As with the long-term rates of sediment generation, sediment yield values are not systematically distributed in the study area (Figure 4b). In addition, sediment yield does not correlate significantly with any metrics we analyzed (Figure 5). This is likely due to the small number of gauging stations included within our study area and noise in the sediment yield record. The strongest correlation is with distance to the first dam, where sediment yield rates are positively correlated with distance to dam. Dams date to as early as the 1950s and sediment yield data from the 1950s-1987 (Lu and Higgitt, 1999). Dams trap sediment and thus will artificially lower sediment yields; a longer distance to dams will thus increase sediment yield from intervening hillslopes. We also see an inverse relationship between sediment yield and basin area due to increased trapping of sediment and overall lower sediment delivery ratios with increasing basin area (Trimble, 1977). Finally, we see a direct relationship between percent agriculture in the upstream watershed and sediment yield. Agriculture typically increases erosion and thus sediment yield, as has been observed elsewhere in China (Schmidt et al., 2017; 2011).

When considering the ratio of long-term rates of sediment generation to short-term rates of sediment yield, ratios range from 2.9 – 9.4 (mean = 5.9±2.8, n = 5); the highest ratio corresponds to the basin with the highest short-term sediment yield and second highest long-term sediment generation rate (Figure 4C). The ratio of modern rates of sediment yield to long-term rates of sediment generation does not have any significant correlations with the parameters considered, although generally the data follow the same patterns as the modern sediment yield

276 data – direct correlations with area in agriculture, distance to the nearest dam, slope, and percent
277 of the basin with landslides and inverse correlations with basin area and mean annual
278 precipitation (Figure 5). In terms of geologic control, we see that slope steepness is directly
279 related to the ratio of modern sediment yield to long-term sediment generation. In terms of
280 human effects on the system, it seems that dams are artificially lowering the modern sediment
281 yield (e.g., Covault et al., 2013; Syvitski et al., 2005) and thus the ratio between modern
282 sediment yield and long-term sediment generation. In contrast, agriculture appears to be
283 generally raising the ratio of modern sediment yield to long-term sediment generation in the
284 study area.

285 Landslides could be entirely a natural geologic control or increased by human activity
286 (deforestation, road building, and agriculture) in the region (Benda and Dunne, 1997). If the
287 landslides were entirely geologic in origin, we would expect the $^{10}Be_i$-derived sediment
288 generation rates to account for these slides because the basins are large enough to integrate the
289 sediment from landslides (Niemi et al., 2005). However, we find a significantly higher modern
290 sediment yield compared to long-term sediment generation. In addition, although the region is
291 classified as a humid temperate climate, there are few trees in the study area. Thus, it appears
292 that landslides in this region are in large part caused by current and/or previous deforestation and
293 agriculture and the effect of landslides in raising sediment yield is a human rather than geologic
294 factor. Thus, we conclude that the ratio of modern sediment yield to long-term sediment
295 generation is driven primarily by human factors.

296 We find that previously modeled RUSLE erosion rates (Jiang et al., 2015) correlate to our
297 new long-term sediment generation rates ($R^2 = 0.51$, $p < 0.05$), but the mean of modelled rates is
298 28 times higher (17-166 times). Similarly, the RUSLE-derived erosion rates are a mean of five

299 times (1.9 to 6.3 times) greater than sediment yield values in the region. Since land use,
300 topography, and precipitation are inputs into the RUSLE model, it is not possible to further
301 explore parameters controlling this ratio – they would be auto-correlated. However, these data
302 suggest that modern hillslope erosion is several times higher than modern sediment yield which
303 is, in turn, several times higher than sediment generation rates.

304 The high rates of modern erosion and sediment yield relative to long-term rates of
305 sediment generation suggest unsustainable erosion in the study area, as previously found in the
306 eastern United States (Reusser et al., 2017). The sediment being eroded off the hillslopes must be
307 accumulating somewhere in the watersheds because it is not all making it to the rivers (Trimble,
308 1977). It seems likely that the sediment is accumulating in reservoirs as well as in terraces,
309 alluvial fans, and toe slope deposits throughout the watershed, a hypothesis confirmed by
310 observations of sediment choked channels and alluvial fans observed in the field (Figure 6).

311 ## 6. Conclusions

312 Using long-term rates of sediment generation from nine tributaries to the lower Jinsha
313 River and sediment yield data from five gauging stations with data from the 1950s-1987 located
314 near those tributaries, we find that the ratio of modern sediment yield to long-term sediment
315 generation is controlled by a mix of agriculture, dams, and landslides in the watersheds.
316 Agricultural activity does not seem to play as large a role in setting those ratios as dams and
317 landslides despite known increase in local erosion due to agriculture. At the basin scale and on
318 short time scales, human activity decreases sediment yield in rivers through dam construction.
319 Slope steepness appears to control long-term rates of sediment generation while the frequency of

landslides, which at least in part are due to human activity in the watershed, controls both the ratio of long-term to modern and the modern sediment yield.

Acknowledgements

The authors would like to thank S. Doak, M. Hill, M. Byerly, L. Leslie, and Y. Wang for assistance in the field. X. Lu provided the modern sediment yield data. The work was funded by an Oberlin College Grant in Aid award to A. H. Schmidt, an Oberlin College Powers Travel Grant to A. H. Schmidt, a National Science Foundation Award to P. R. Bierman (NSF-EAR-1114159), and the Program of Introducing Talents of Discipline to Universities or "111 Project" of China award to Y. Tang (B08037). This work was performed under the auspices of the U.S. Department of Energy by Lawrence Livermore National Laboratory under Contract DE-AC52-07NA27344. This is LLNL-JRNL-751018.

Reference List

Andermann, C., Bonnet, S., and Gloaguen, R., 2011, Evaluation of precipitation data sets along the Himalayan front: Geochemistry, Geophysics, Geosystems, v. 12, no. 7, p. Q07023.

Balco, G., Stone, J. O., Lifton, N. A., and Dunai, T. J., 2008, A complete and easily accessible means of calculating surface exposure ages or erosion rates from ^{10}Be and ^{26}Al measurements: Quaternary Geochronology, v. 3, p. 174-195.

Benda, L., and Dunne, T., 1997, Stochastic forcing of sediment supply to channel networks from landsliding and debris flow: Water Resources Research, v. 33, no. 12, p. 2849-2863.

Bierman, P. R., Howe, J., Stanley-Mann, E., Peabody, M., Hilke, J., and Massey, C. A., 2005, Old images record landscape change through time: GSA Today, v. 15, no. 4, p. 4-10.

Bierman, P. R., and Steig, E. J., 1996, Estimating rates of denudation using cosmogenic isotope abundances in sediment: Earth Surface Processes and Landforms, v. 21, p. 125-139.

Brown, E. T., Stallard, R. F., Larsen, M. C., Raisbeck, G. M., and Yiou, F., 1995, Denudation rates determined from the accumulation of in-situ produced ^{10}Be in the Luquillo Experimental Forest, Puerto Rico: Earth and Planetary Science Letters, v. 129, p. 193-202.

Brown, L., Pavich, M. J., Hickman, R. E., Klein, J., and Middleton, R., 1988, Erosion of the Eastern United States observed with ^{10}Be: Earth Surface Processes and Landforms, v. 13, p. 441-457.

Burchfiel, B. C., and Chen, Z., 2012, Tectonics of the Southeastern Tibetan Plateau and its adjacent foreland (Vol. 210), Boulder, CO, The Geological Society of America.

Chappell, J., Zheng, H. B., and Fifield, K., 2006, Yangtse River sediments and erosion rates from source to sink traced with cosmogenic Be-10: Sediments from major rivers: Palaeogeography Palaeoclimatology Palaeoecology, v. 241, no. 1, p. 79-94.

Chen, J., Chen, J., Liao, A., Cao, X., Chen, L., He, C., Han, G., Peng, S., Lu, M., Zhang, W., Tong, X., and Mills, J., 2015, Global land cover mapping at 30 m resolution: A POK-based operational approach: ISPRS Journal of Photogrammetry and Remote Sensing, v. 103, p. 7-27.

Corbett, L. B., Bierman, P. R., and Rood, D. H., 2016, An approach for optimizing *in situ* cosmogenic ^{10}Be sample preparation: Quaternary Geochronology, v. 33, p. 24-34.

Covault, J. A., Craddock, W. H., Romans, B. W., Fildani, A., and Gosai, M., 2013, Spatial and temporal variations in landscape evolution: Historic and longer-term sediment flux through global catchments: Journal of Geology, v. 121, no. 1, p. 35-56.

Granger, D. E., Kirchner, J. W., and Finkel, R. C., 1996, Spatially averaged long-term erosion rates measured from in-situ produced cosmogenic nuclides in alluvial sediment: The Journal of Geology, v. 104, p. 249-257.

Hewawasam, T., Von Blanckenburg, F., Schaller, M., and Kubik, P. W., 2003, Increase of human over natural erosion rates in tropical highlands constrained by cosmogenic nuclides: Geology, v. 33, no. 7, p. 597-600.

Jiang, L., Yao, Z., Liu, Z., Wu, S., Wang, R., and Wang, L., 2015, Estimation of soil erosion in some sections of Lower Jinsha River based on RUSLE: Natural Hazards, v. 76, no. 3, p. 1831-1847.

Jull, A. J. T., Scott, E. M., and Bierman, P., 2015, The CRONUS-Earth inter-comparison for cosmogenic isotope analysis: Quaternary Geochronology, v. 26, p. 3-10.

Kirchner, J. W., Finkel, R., C., Riebe, C. S., Granger, D. E., Clayton, J. L., King, J. G., and Megahan, W. F., 2001, Mountain erosion over 10 yr, 10 k.y., and 10 m.y. time scales: Geology v. 29, no. 7, p. 591-594.

Kohl, C. P., and Nishiizumi, K., 1992, Chemical isolation of quartz for measurement of in-situ produced cosmogenic nuclides: Geochimica et Cosmochimica Acta, v. 56, p. 3583-3587.

Lal, D., 1991, Cosmic ray labeling of erosion surfaces: *in situ* nuclide production rates and erosion models: Earth and Planetary Science Letters, v. 104, p. 424-439.

Lu, X., 2005, Spatial variability and temporal change of water discharge and sediment flux in the lower Jinsha tributary: impact of environmental changes: River Research and Applications, v. 21, no. 2 - 3, p. 229-243.
Lu, X. X., and Higgitt, D. L., 1998, Recent changes of sediment yield in the Upper Yangtze, China: Environmental Management, v. 22, no. 5, p. 697-709.
-, 1999, Sediment yield variability in the Upper Yangtze, China: Earth Surface Processes and Landforms, v. 24, no. 12, p. 1077-1093.
Matmon, A., Bierman, P. R., Larsen, J., Southworth, S., Pavich, M. J., Finkel, R. C., and Caffee, M. W., 2003, Erosion of an ancient mountain range, the Great Smoky Mountains, North Carolina and Tennessee: American Journal of Science, v. 303, p. 517-855.
NASA LP-DAAC, 2012, ASTER GDEM, *in* NASA Land Processes Distributed Active Archive Center (LP DAAC), ed., LP DAAC.
National Research Council, 2010, Landscapes on the edge: New horizons for research on Earth's surface, national academies Press.
Niemi, N. A., Oskin, M., Burbank, D. W., Heimsath, A. M., and Gabet, E. J., 2005, Effects of bedrock landslides on cosmogenically determined erosion rates: Earth and Planetary Science Letters, v. 237, p. 480-498.
Nishiizumi, K., Imamura, M., Caffee, M. W., Southon, J. R., Finkel, R. C., and McAninch, J., 2007, Absolute calibration of ^{10}Be AMS standards: Nuclear Instruments and Methods B, v. 258, no. 2, p. 403-413.
Peel, M. C., Finlayson, B. L., and McMahon, T. A., 2007, Updated world map of the Koppen-Geiger climate classification: Hydrology and Earth System Sciences, v. 11, no. 5, p. 1633-1644.
Portenga, E. W., and Bierman, P. R., 2011, Understanding Earth's eroding surface with ^{10}Be: GSA Today, v. 21, no. 8, p. 4-10.
Portenga, E. W., Bierman, P. R., Duncan, C., Corbett, L. B., Kehrwald, N. M., and Rood, D. H., 2015, Erosion rate of the Bhutanese Himalaya determined using *in situ*-produced ^{10}Be: Geomorphology, v. 233, p. 112-126.
Reusser, L. J., Bierman, P. R., Rizzo, D. M., Portenga, E. W., and Rood, D. H., 2017, Characterizing landscape-scale erosion using ^{10}Be in detrital fluvial sediment: Slope-based sampling strategy detects the effect of widespread dams: Water Resources Research, v. 53.
Reusser, L. J., Bierman, P. R., and Rood, D. H., 2015, Quantifying human impacts on rates of erosion and sediment transport at a landscape scale: Geology v. 43, no. 2, p. 171-174.
Schmidt, A. H., Gonzalez, V. S., Bierman, P. R., Neilson, T. B., and Rood, D. H., 2017, Agricultural land use doubled sediment loads in western China's rivers: Anthropocene.
Schmidt, A. H., Montgomery, D. R., Huntington, K. W., and Liang, C., 2011, The question of communist land degradation: New evidence from local erosion and basin-wide sediment yield in Southwest China and Southeast Tibet: Annals of the Association of American Geographers, v. 101, no. 3, p. 1-20.
Schmidt, A. H., Neilson, T. B., Bierman, P. R., Rood, D. H., Ouimet, W. B., and Sosa Gonzalez, V., 2016, Influence of topography and human activity on apparent *in situ* ^{10}Be-derived erosion rates in Yunnan, SW China: Earth Surface Dynamics, v. 4, no. 4, p. 819-830.
Stone, J. O., 2000, Air pressure and cosmogenic isotope production: Journal of Geophysical Research, v. 105, no. B10, p. 23,573-523,579.
Syvitski, J. P. M., Vorosmarty, C. J., Kettner, A. J., and Green, P., 2005, Impact of humans on the flux of terrestrial sediment to the global coastal ocean: Science, v. 308, no. 5720, p. 376-380.
Tomkins, K., Humphreys, G., Wilkinson, M., Fink, D., Hesse, P., Doerr, S., Shakesby, R., Wallbrink, P., and Blake, W., 2007, Contemporary versus long - term denudation along a passive plate margin: the role of extreme events: Earth Surface Processes and Landforms, v. 32, no. 7, p. 1013-1031.

Trac, C. J., Harrell, S., Hinckley, T. M., and Henck, A. C., 2007, Reforestation programs in Southwest China: Reported success, observed failures, and the reasons why: Journal of Mountain Science, v. 4, no. 4, p. 275-292.

Trac, C. J., Schmidt, A. H., Harrell, S., and Hinckley, T. M., 2013, Is the returning farmland to forest program a success? Three case studies from Sichuan: Environmental Practice, v. 15, no. 3, p. 350-366.

Trimble, S. W., 1977, Fallacy of Stream Equilibrium in Contemporary Denudation Studies: American Journal of Science, v. 277, no. 7, p. 876-887.

Urgenson, L. S., Hagmann, R. K., Henck, A. C., Harrell, S., Hinckley, T. M., Shepler, S. J., Grub, B. L., and Chi, P. M., 2010, Social-ecological resilience of a Nuosu community-linked watershed, southwest Sichuan, China: Ecology and Society, v. 15, no. 4, p. 2.

Vanacker, V., Von Blanckenburg, F., Govers, G., Molina, A., Poesen, J., Deckers, J., and Kubik, P., 2007, Restoring dense vegetation can slow mountain erosion to near natural benchmark levels: Geology v. 35, no. 4, p. 303-306.

Vanmaercke, M., Poesen, J., Govers, G., and Verstraeten, G., 2015, Quantifying human impacts on catchment sediment yield: A continental approach: Global and Planetary Change, v. 130, p. 22-36.

Von Blanckenburg, F., Hewawasam, T., and Kubik, P. W., 2004, Cosmogenic nuclide evidence for low weathering and denudation in the wet, tropical highlands of Sri Lanka: Journal of Geophysical Research: Earth Surface, v. 109, no. F3, p. F03008.

Wittmann, H., von Blanckenburg, F., Maurice, L., Guyot, J. L., Filizola, N., and Kubik, P. W., 2011, Sediment production and delivery in the Amazon River basin quantified by *in situ*-produced cosmogenic nuclides and recent river loads: Geological Society of America Bulletin, v. 123, no. 5-6, p. 934-950.

Wu, Y., Liu, X., Liu, L., and Shi, P., 2016, Landslide and Debris Flow Disasters in China, Natural Disasters in China, Springer, p. 73-101.

Yatagai, A., Kamiguchi, K., Arakawa, O., Hamada, A., Yasutomi, N., and Kitoh, A., 2012, APHRODITE: Constructing a long-term daily gridded precipitation dataset for Asia based on a dense network of rain gauges: Bulleting of the American Meteorological Society, v. 39, no. 9, p. 1401-1415.

Yao, Y.H., Zhang, B.P., Ma, X.D., and Ma, P., 2006, Large-scale hydroelectric projects and mountain development on the upper Yangtze river: Mountain Research and Development, v. 26, no. 2, p. 109-114.

Zhou, G. G., Ouyang, C., and Chen, X., 2016, Key Laboratory of Mountain Hazards and Earth Surface Processes, Chinese Academy of Sciences: Mountain Research and Development, v. 36, no. 1, p. 116-118.

Figure captions

Figure 1: (A) Location of the study area in Asia. (B) Distribution of rainfall (Yatagai et al., 2012), sample sites, first dams, and basin boundaries in the study area. Italicized numbers and letters show approximate location of pictures in figures 2 and 6. (C) Slopes in the study area (NASA LP-DAAC, 2012). (D) Carbonate rocks (large orange shapes) (Burchfiel and Chen, 2012) and landslides (small purple shapes) in the study basins. (E) Land use throughout the study area and surrounding region (Chen et al., 2015).

Figure 2: Photos of the field sites going from upstream (A) to downstream (D) that show the increasing incision in the landscape due to the upstream propagation of knickpoints. (A) Photo taken at site JS09. (B) Photo taken from sample JS06 towards main stem of the Jinsha. (C) Photo taken of main stem of the Jinsha from road between samples JS03 and JS04. The cliffs seen are only a few meters tall on the main stem of the Jinsha near sample JS05. (D) Photo taken near sample JS03. Approximate location of photos shown in figure 1B.

Figure 3: Long profiles of the main stem (black) and sampled tributaries (grey) showing the location of the main stem knickpoint. Profiles are smoothed using a kernel smoothing algorithm.

Figure 4: Maps showing (A) long-term sediment generation rates, (B) modern sediment yield rates (Lu and Higgitt, 1998, 1999), and (C) the ratio of sediment yield to sediment generation.

Figure 5: Correlations between measures of erosion (from top to bottom: sediment generation rate, sediment yield rate, and the ratio of sediment yield to sediment generation) as a function of basin average parameters (from left to right: % agriculture in the basin, basin area, distance to first dam, % landslides in the upstream basin, mean slope of the basin, and mean annual precipitation). All correlations discussed are detailed in table DR5.

Figure 6: Pictures in the study area showing the vegetation, landslides, and sediment storage. (A) Large rocks, small toe slope storage, and bare hillslopes near JS07; (B) Shallow landslides, deforested hillslopes, and sediment storage near JS11; (C) In channel sediment storage near JS05; (D) Alluvial fan and sediment storage in the main stem of the Jinsha near JS05; (E) Shallow landsliding and in channel sediment storage at JS08; (F) Shallow landsliding, bare hillslopes, and in channel sediment storage near JS08. Approximate photo locations shown on figure 1B.

Figure 1

Click here to download high resolution image

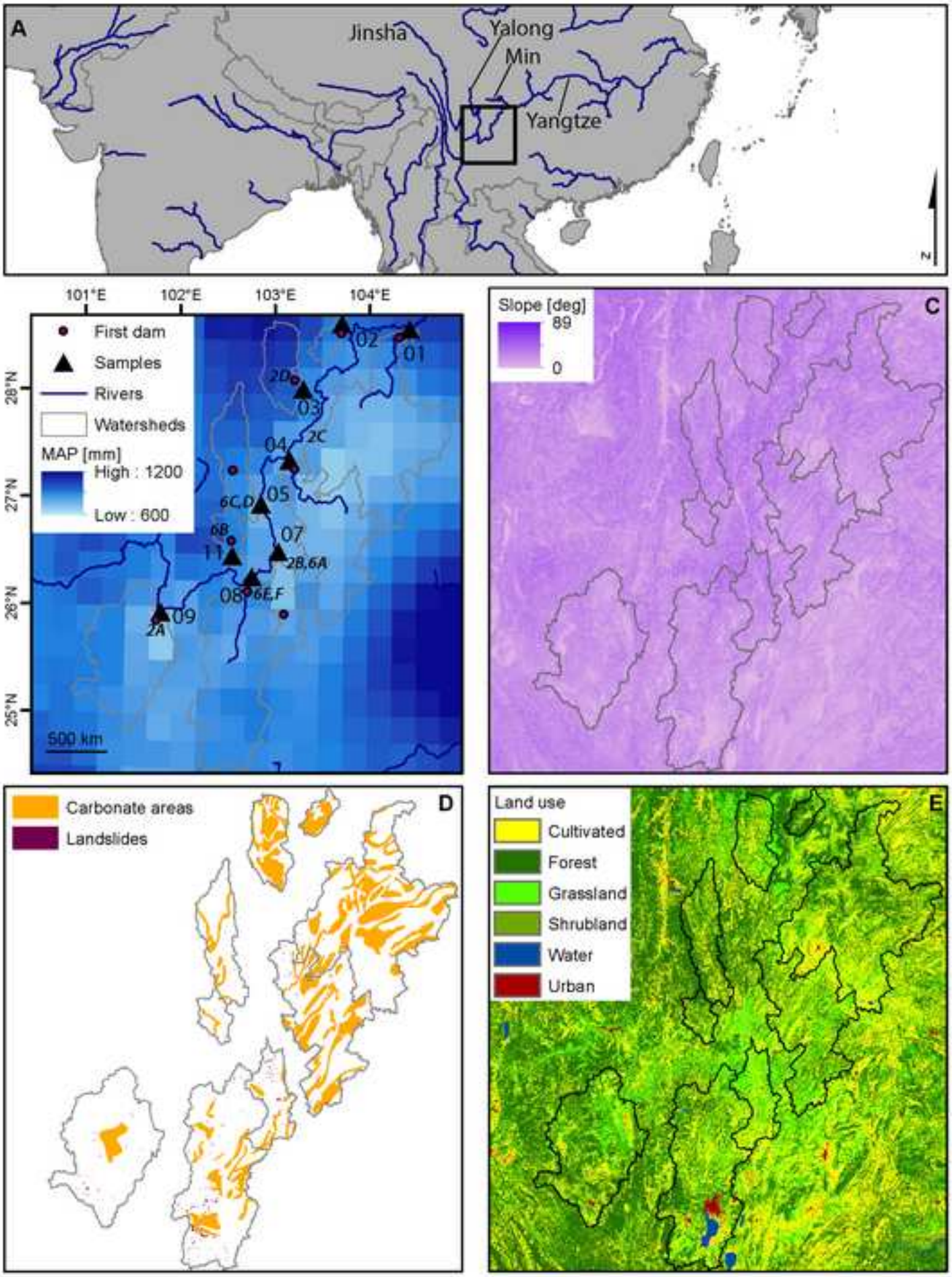

Figure 2

Click here to download high resolution image

Figure 3

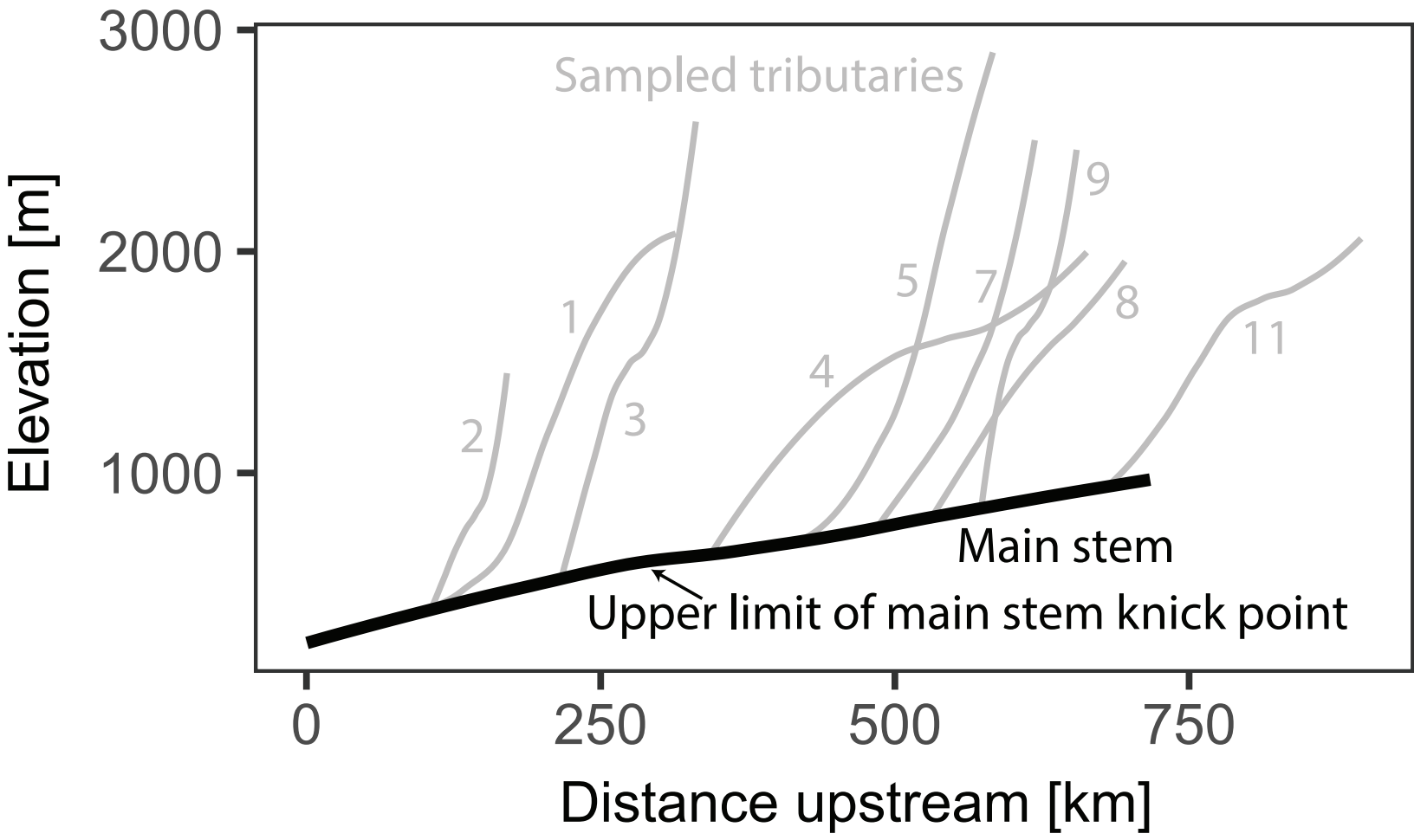
3000
2000
1000
Elevation [m]
Sampled tributaries
1
2
3
4
5
7
8
9
11
Main stem
Upper limit of main stem knick point
0
250
500
750
Distance upstream [km]

Figure 4

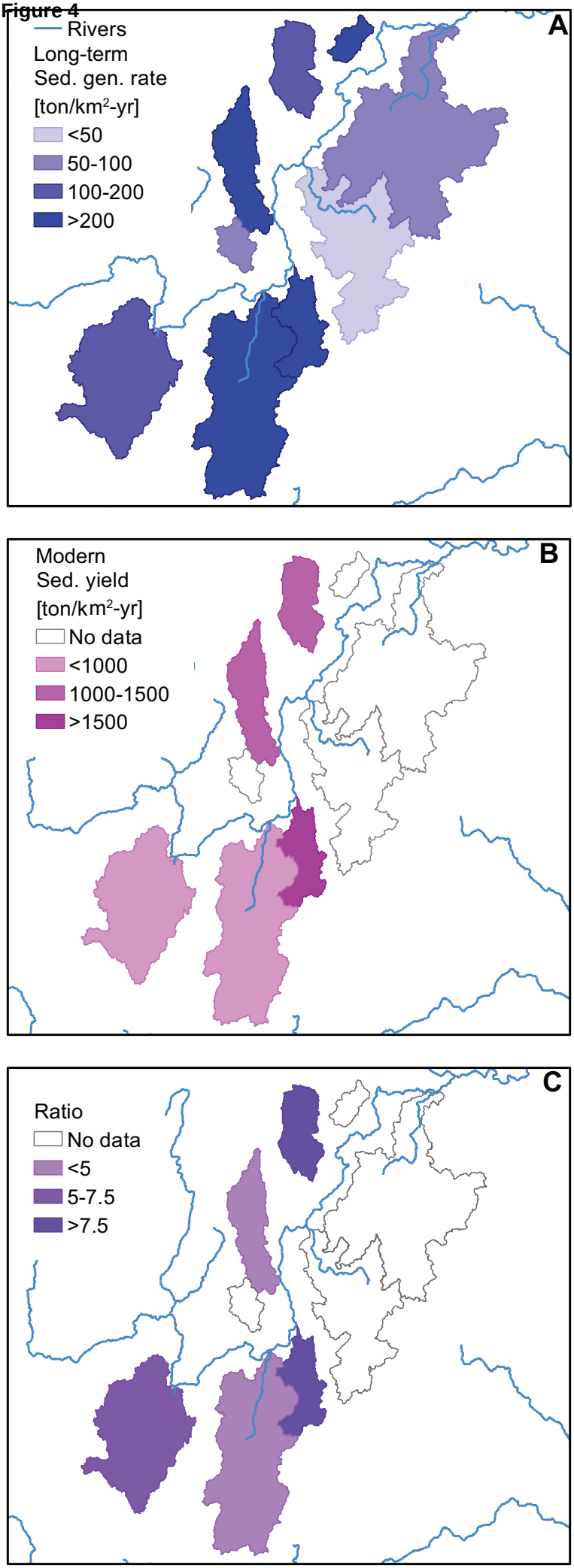
Rivers
Long-term
Sed. gen. rate
[ton/km²-yr]
<50
50-100
100-200
>200
A
Modern
Sed. yield
[ton/km²-yr]
No data
<1000
1000-1500
>1500
B
Ratio
No data
<5
5-7.5
>7.5
C

Figure 5

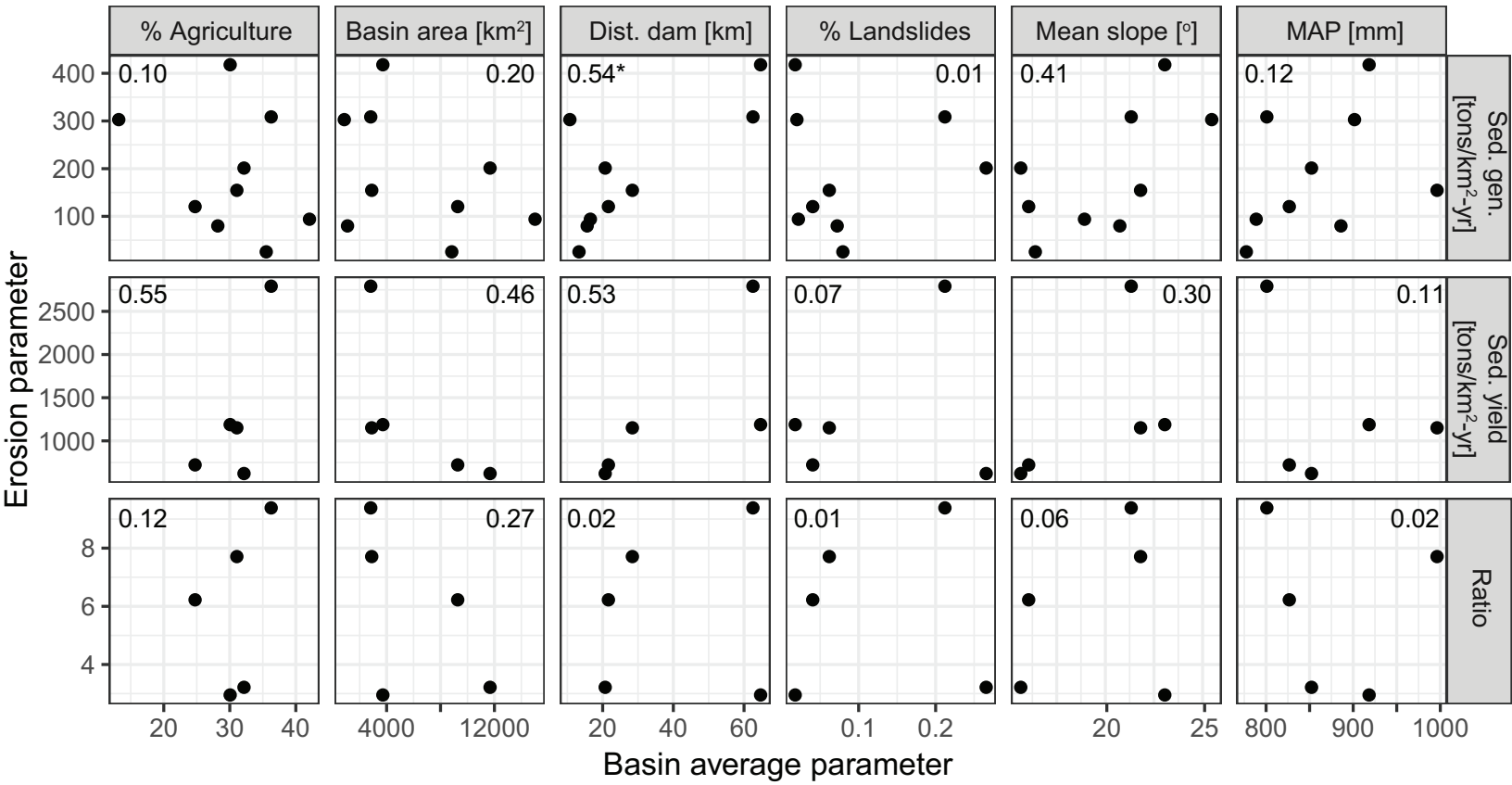
% Agriculture
Basin area [km²]
Dist. dam [km]
% Landslides
Mean slope [°]
MAP [mm]
Sed. gen. [tons/km²-yr]
Sed. yield [tons/km²-yr]
Ratio
0.10
0.20
0.54*
0.01
0.41
0.12
0.55
0.46
0.53
0.07
0.30
0.11
0.12
0.27
0.02
0.01
0.06
0.02
Erosion parameter
Basin average parameter

Figure 6

Click here to download high resolution image